Sea Surface Temperature Feedback Extends the Predictability of Tropical Intraseasonal Oscillation

XIOUHUA FU AND BO YANG

International Pacific Research Center, School of Ocean and Earth Science and Technology, University of Hawaii at Manoa, Honolulu, Hawaii

QING BAO

Institute of Atmospheric Physics, Chinese Academy of Sciences, Beijing, China

BIN WANG

International Pacific Research Center, and Department of Meteorology, School of Ocean and Earth Science and Technology, University of Hawaii at Manoa, Honolulu, Hawaii

(Manuscript received 9 February 2007, in final form 13 April 2007)

ABSTRACT

The possible impacts of different sea surface temperature (SST) configurations on the predictability of the boreal summer tropical intraseasonal oscillation (TISO) are assessed with a series of ensemble forecasts. The five different lower boundary conditions examined in this study are, respectively, (i) the fully interactive ocean–atmosphere coupling, (ii) "smoothed" SST, which excludes the intraseasonal signal from sea surface forcing, (iii) damped persistent SST, (iv) coupling to a slab mixed-layer ocean, and (v) daily SST from the coupled forecast. The full atmosphere–ocean coupling generates an interactive SST that results in the highest TISO predictability of about 30 days over Southeast Asia. The atmosphere-only model is capable of reaching this predictability if the ensemble mean daily SST forecast by the coupled model is used as the lower boundary condition, which suggests that, in principle, the so-called tier-one and tier-two systems have the same predictability for the boreal summer TISO. The atmosphere-only model driven by either smoothed or damped persistent SSTs, however, has the lowest predictability (~20 days). The atmospheric model coupled to a slab mixed-layer ocean achieves a predictability of 25 days. The positive SST anomalies in the northern Indo–western Pacific Oceans trigger convective disturbances by moistening and warming up the atmospheric boundary layer. The seasonal mean easterly shear intensifies the anomalous convection by enhancing the surface convergence. An overturning meridional circulation driven by the off-equatorial anomalous convection suppresses the near-equatorial convection and enhances the northward flows, which further intensify the off-equatorial surface convergence and the TISO-related convection. Thus, the boreal summer mean easterly shear and the overturning meridional circulation in the northern Indo–western Pacific sector act as "amplifiers" for the SST feedback to the convection of the TISO.

1. Introduction

The tropical intraseasonal oscillation (TISO) is a prominent climate variability that originates in the tropics and has its impacts all over the globe (Lau and Waliser 2005; Donald et al. 2006). The strongest atmospheric and oceanic disturbances associated with the TISO (e.g., atmospheric convection and sea surface temperature) are observed in the tropical Indo–western Pacific warm-pool region (Madden and Julian 1972; Lau and Chan 1986; Krishnamurti et al. 1988; Wang and Rui 1990; Zhang 1996), which often propagates poleward to regulate the wet and dry spells of monsoons in the Asian and Australian continents (Yasunari 1979; Sikka and Gadgil 1980; Wang and Rui 1990; Hendon and Liebmann 1990). The TISO-related surface winds produce considerable fluctuations of thermocline and upper-ocean currents in the equatorial Indian (Han et al. 2004) and Pacific Oceans (Kessler et al. 1995). The

latter are postulated to play a significant role in the initiation and growth of El Niño (McPhaden 2004; Seo and Xue 2005). The convection associated with TISO also impacts the rainfall variability over North and South America (Mo 2000; Paegle et al. 2000; Whitaker and Weickmann 2001; Jones et al. 2004; Ding and Wang 2005) through tropical–extratropical teleconnection (Ferranti et al. 1990). Because of the downscale modulations of TISO on synoptic weather (Maloney and Hartmann 2000; Goswami et al. 2003; Bessafi and Wheeler 2006) and the upscale influences of TISO on interannual-to-interdecadal variability (Timmermann and Jin 2002), improving prediction of TISO has the potential to advance the forecast skills of both weather and climate variability.

The recurrent nature of TISO, with a period of 20–90 days, does offer an opportunity to predict the weather envelope beyond 2 weeks (Waliser et al. 2006). This will bridge the gap between the weather forecast (within 1 week) and seasonal outlook (beyond 1 month), making the so-called seamless forecast possible. As reflected in the historic progress of weather forecast and seasonal prediction, statistical models are proven to be useful tools in the forecast of TISO. Several statistical predictive models have shown certain useful skills up to 15–20-day lead time (Waliser et al. 2006; Goswami and Xavier 2003; Webster and Hoyos 2004). On the other hand, the predictive skill of the TISO in the dynamical forecast models, for example, an old version (Hendon et al. 2000; Jones et al. 2000) or the latest version (Seo et al. 2005) of the National Centers for Environmental Prediction (NCEP) models, is only about 7–10 days when SSTs are fixed on climatology. The relatively short forecast skill of dynamic models indicates that the representation of TISO requires further improvements (Lin et al. 2006). At the same time, the possible impacts of initial and boundary conditions on the TISO predictability and prediction need to be explored (Krishnamurti et al. 1992; Reichler and Roads 2005). The outcomes can provide useful guidance for both the TISO hindcasts and operational forecasts.

Fu et al. (2007) assessed the potential impact of interactive air–sea coupling on the TISO predictability. In that study, 20 TISO events during 15 boreal summers were selected from a coupled control run as forecast targets. A series of "twin" perturbation experiments (Lorenz 1982; Waliser et al. 2003a) were carried out for all events under two different boundary conditions. In the coupled forecasts, underlying SST was directly determined by the interactive air–sea coupling. In the uncoupled forecasts, the lower boundary condition was specified as the "smoothed" SST[1] from the coupled control run. These two groups of forecasts used both the same initial atmospheric conditions and the same atmospheric model. If the evolutions of the TISO were primarily governed by internal atmospheric dynamics, the difference of TISO predictability between these two forecasts should be indistinguishable, and the intraseasonal SST anomaly generated in the coupled system should be basically a passive response to the TISO atmospheric forcing. The results of Fu et al. (2007), however, turn out to be quite different. They found that the TISO predictability in the coupled forecasts is significantly higher than that in the uncoupled forecasts over the tropical Asian–western Pacific region (10°S–30°N, 60°–160°E). In the uncoupled case, the TISO-related rainfall predictability is only about 17 days, averaged over the tropical Asian–western Pacific. The predictability increases to 24 days after including the effects of intraseasonally varying SSTs in the coupled forecasts.

As pointed out in Waliser et al. (2003b) and Fu et al. (2007), in order to thoroughly understand the impacts of different SST configurations on the TISO predictability, a few more sensitivity experiments should be conducted. In this study, the following five different SST settings were examined: (i) the fully interactive ocean–atmosphere coupling (CPL), (ii) smoothed SST, which excludes intraseasonal surface forcing (ATM), (iii) damped persistent SST (ATMp), (iv) SST coupled to a slab mixed-layer ocean (ATMf), and (v) daily SST from the coupled forecast run (ATMd). A more detailed description of these experiments is given in Table 1. Instead of performing twin perturbation experiments for many TISO events, as in Waliser et al. (2003a) and Fu et al. (2007), we will select only few events in this study and carry out a large number of ensemble forecasts as in Tracton and Kalnay (1993) and Liess et al. (2005).

The major objectives of this study are as follows: (i) quantify the possible impacts of different SST configurations on the TISO predictability and identify an optimal way to set up lower boundary conditions for TISO hindcasts and operational forecasts, and (ii) understand the physical processes responsible for the predictability differences among various SST configurations. The questions to be addressed include (a) to what degree is the TISO predictability affected by different lower boundary conditions; and (b) why does predictability differ among these runs, particularly between the

---

[1] The smoothed SST means that the intraseasonal variability (20–90 days) in the daily SST of the coupled control run was removed to exclude the intraseasonal forcing from the underlying sea surface.

TABLE 1. Ensemble forecasts under five different SST configurations.

Expt name	SSTs used during 90-day forecasts
CPL	Forecast directly by the interactive air–sea coupling
ATM	The daily SST from the coupled control run with 20–90-day variability removed (referred to as smoothed SST)
ATMp	The daily SST from the coupled control run is linearly interpolated to the smoothed SST during first 10-day forecast (referred to as damped persistent SST)
ATMf	The SST anomaly derived from coupling to a slab mixed-layer ocean (with a depth of 30 m) is added to the smoothed SST
ATMd	The ensemble mean daily SST from the CPL forecasts

coupled forecast (CPL) and atmosphere-only forecast driven by smoothed SST (ATM)?

The coupled model used to address the above questions is introduced in section 2, along with the ensemble experimental designs and the methods used to quantify the predictability. Section 3 compares the TISO predictability under different lower boundary conditions. Section 4 is devoted to unraveling the physical processes through which the intraseasonal SST anomaly feeds back to the TISO, thus resulting in an extension of the predictability. In the last section, major findings of this study are summarized and future research directions are proposed.

2. Model and methodology

a. Model

The coupled model used in this study comprises an atmospheric general circulation model (AGCM) and an intermediate ocean model with full coupling. The atmospheric model is the ECHAM4 AGCM (Roeckner et al. 1996). Its horizontal resolution is about 3.75° in both longitude and latitude, with 19 vertical levels extending from the surface to 10 hPa. The mass flux scheme of Tiedtke (1989) with a CAPE closure (Nordeng 1994) is used to parameterize the deep, shallow, and midlevel convection.

The ocean component of the coupled model is a 2½-layer tropical upper-ocean model with a horizontal resolution of 0.5° in both longitude and latitude. It was originally developed by Wang et al. (1995) and improved by Fu and Wang (2001), who combine the mixed-layer thermodynamics of Gaspar (1988) with the upper-ocean dynamics of McCreary and Yu (1992). The entrained water temperature is parameterized as a function of thermocline depth, like the one used in Zebiak and Cane (1987) and Jin (1996).

The ECHAM4 AGCM and the ocean model are coupled in the tropical Indo–Pacific Oceans (30°S–30°N) without explicit heat flux correction. Outside the coupled region, the underlying SST is specified as the climatological monthly mean SST averaged for 16 yr (1979–94) from the boundary conditions of the second Atmospheric Model Intercomparison Project (AMIP-II) experiments. The atmospheric component exchanges information with the ocean component once per day. The initial atmospheric state is a restart file on 1 January from a long-term atmosphere-only integration. The initial ocean condition is the January state after a 10-yr integration of the stand-alone ocean model forced by observed climatological surface winds and heat fluxes.

This so-called hybrid ocean–atmosphere coupled model much better simulates monsoon climatology in the Asian–western Pacific region relative to the stand-alone ECHAM4 AGCM (Fu et al. 2002). It also produces a TISO that mimics the one existing in the observations (Kemball-Cook et al. 2002; Fu et al. 2003; Fu and Wang 2004b), with coherent spatiotemporal evolutions of rainfall, surface winds, and SST, and a realistic intensity and period (or propagating speed). As demonstrated in Fu et al. (2007), this hybrid coupled model is a very useful tool for studying the TISO predictability.

b. Experimental designs

A new strategy, which is different from that used in Fu et al. (2007), has been adopted to carry out the ensemble experiments. In the previous study, 20 events were selected. A total of 160 ensembles (2 initial-conditions × 4 phases × 20 events) were carried out for each SST configuration. In this study, only two TISO events are targeted (one is strong, the other is weak). They are, respectively, from year 10 and 20 of the coupled control run (see Fig. 2 in Fu et al. 2007). Eighty ensembles (10 initial-conditions × 4 phases × 2 events) were conducted for each SST scenario. In fact, after comparing the major results (as presented in Fu et al. 2007) derived with these two different ensemble approaches, very similar conclusions were reached (figures not shown). Considering that we have five different SST configurations to be examined, the latter

method is apparently more practical because of the greatly reduced computational cost per SST setting.

Prior to conducting the ensemble forecasts, four phases [i.e., break (phase I), break to active (phase II), active (phase III), and active to break (phase IV)] of the selected events were identified from the daily time series of the filtered rainfall averaged in the eastern Indian Ocean (EIO; 5°S–5°N, 80°–100°E). Then, 10 ensemble forecasts were carried out and started from each phase of the selected events. The perturbed initial conditions of the ensembles were generated by adding day-to-day root-mean-square differences of four prognostic variables (u, v, T, q) within the specific month onto the original initial conditions as in Waliser et al. (2003a) and Fu et al. (2007). Each ensemble forecast was integrated for 90 days. To extract the intraseasonal variability and distinguish its predictability from synoptic weather, 120-day output from the control run before the initial time was concatenated to the 90-day forecast. Finally, a bandpass filter was used on the 210-day time series to extract the 20–90-day intraseasonal variability.

c. Measures of predictability

To quantify the impacts of different SST configurations on the predictability of the TISO, two complementary measures of predictability (Fu et al. 2007) were used in this study. One is the ratio of the signal to forecast error (Waliser et al. 2003a), and the other is the anomalous correlation coefficient (ACC; Hollingsworth et al. 1980). In the first approach, the signal of a given TISO event is defined as the variance of its intraseasonal variability averaged within a sliding window that is large enough to encompass a TISO event (Goswami and Xavier 2003). The forecast error is defined as the variance of the difference between the perturbed forecast and the target event. The signal-to-error ratio is calculated at individual grid points and gives a spatial distribution of the TISO predictability. In the second approach, the ACC is calculated over a specific domain to quantify the spatial similarity of two fields. Given that the TISO exhibits coherent spatiotemporal evolutions in the Asian–western Pacific region, the ACC offers a measure complementary to the pointwise signal-to-error ratio.

3. Predictability under different lower boundary conditions

a. Coupled versus uncoupled

Even without processing the forecasts with any filtering or statistics, the impacts of air–sea coupling on the TISO predictability can be clearly seen from the fore-cast rainfall evolutions under two different boundary conditions. Figure 1 shows the latitude–time cross sections of two selected TISO events and the 10-ensemble-mean forecasts with the coupled model (CPL) and the uncoupled model (ATM). All results have been averaged between 65° and 120°E, which is a longitudinal band where the TISO shows prominent northward propagation in boreal summer (Yasunari 1979; Lau and Chan 1986; Wang and Rui 1990). The forecasts start from phase I of the selected events, with the dry spells close to the equator and the wet spells around 15°N. For event one (Fig. 1a), the coupled model predicts the northward progression of the dry spell well, which is initially near the equator and propagates to about 15°N at day 25 (Fig. 1b). However, the dry spell forecast by the atmospheric model only propagates to 10°N on day 10, staying there until day 40 (Fig. 1c). The associated equatorial rainfall tends to last much longer than that in both the coupled control run (Fig. 1a) and the coupled forecast (Fig. 1b). For event two, the coupled model predicts not only the northward-propagating dry spell well, but also the follow-up wet spell and the standing rainfall around 15°N from day 30 to 40 (Figs. 1d,e). For the atmosphere-only model, the forecast rainfall (Fig. 1f) quickly diverges from the target (Fig. 1d) following day 15. The northward propagation of the dry spell is apparently slower, and so is the follow-up wet spell. The causes of these differences and the possible implication on the TISO period will be discussed later. Nevertheless, these results clearly illustrate that the coupled model (Figs. 1b,e) has longer predictability than the atmosphere-only model driven by the smoothed SST (Figs. 1c,f).

To quantify the TISO predictability with the ratio of signal to forecast error, the TISO signal is estimated as the variance of the filtered rainfall from the control run subject to a 51-day running mean. The forecast error is calculated as the variance of difference between an individual forecast and the control run. Figure 2 presents the averaged signal and forecast error[2] over Southeast Asia (10°–30°N, 65°–120°E) for the forecasts under two different SST configurations and starting from four different phases, respectively. While the predictability is defined as the day when the error is equal to the signal, the TISO predictability is the highest when forecasts start from phase I (Fig. 2a). Referring back to the rainfall spatial distributions at four start phases (Fig. 4 in Fu et al. 2007), phase I (III) corresponds to the wet (dry) phase over Southeast Asia and phase II (IV) is the

---

[2] The nonzero errors before the start of all forecasts are due to the use of filtering.
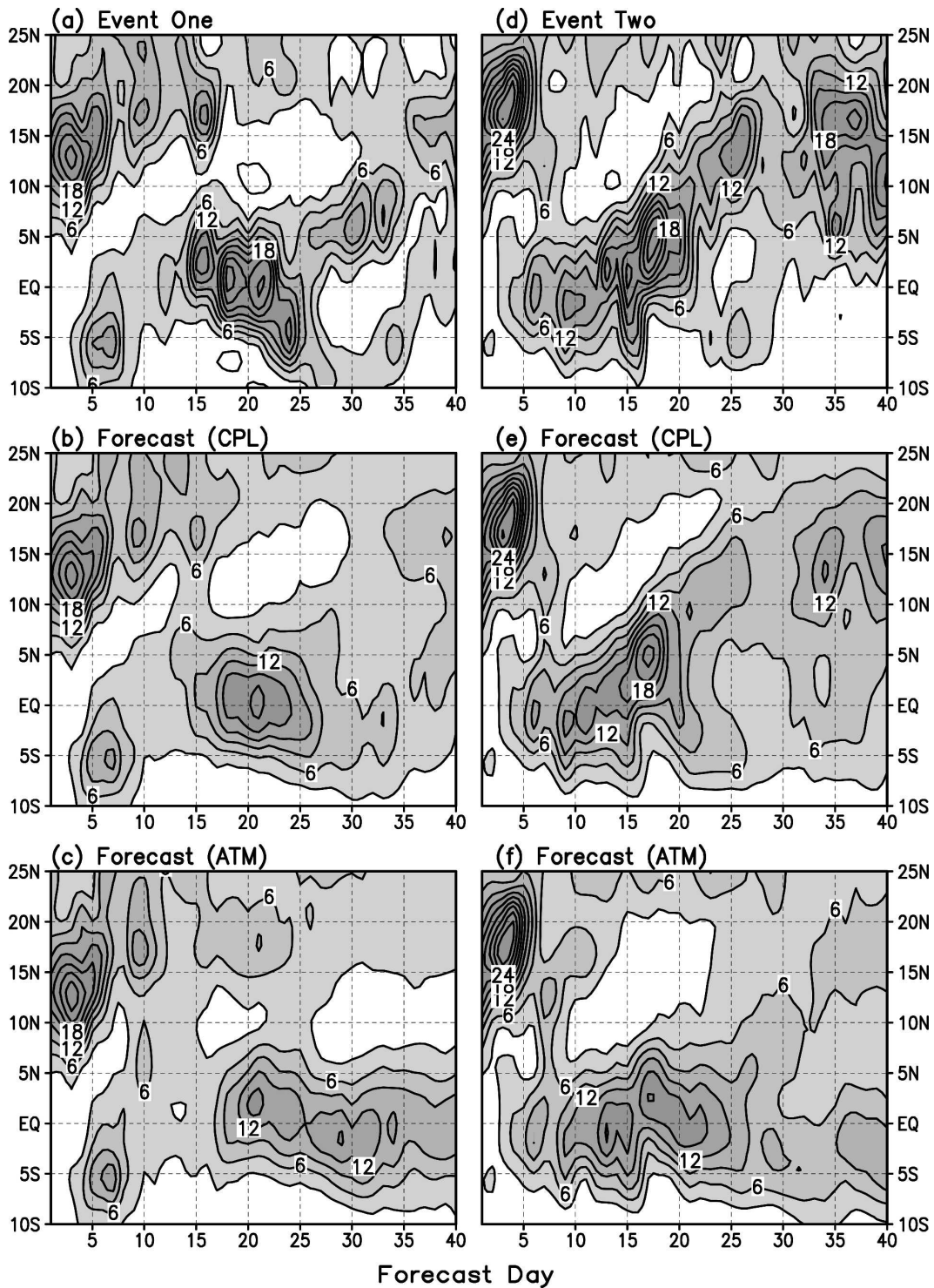
FIG. 1. Two selected TISO events: event (left) one and (right) two. The (a),(d) latitude–time cross sections of rainfall averaged over 65°–120°E, (b),(e) ensemble mean forecasts with the coupled model (CPL), and (c),(f) the atmosphere-only model forced by smoothed SST (ATM). Contour interval is 3 mm day^{-1}.
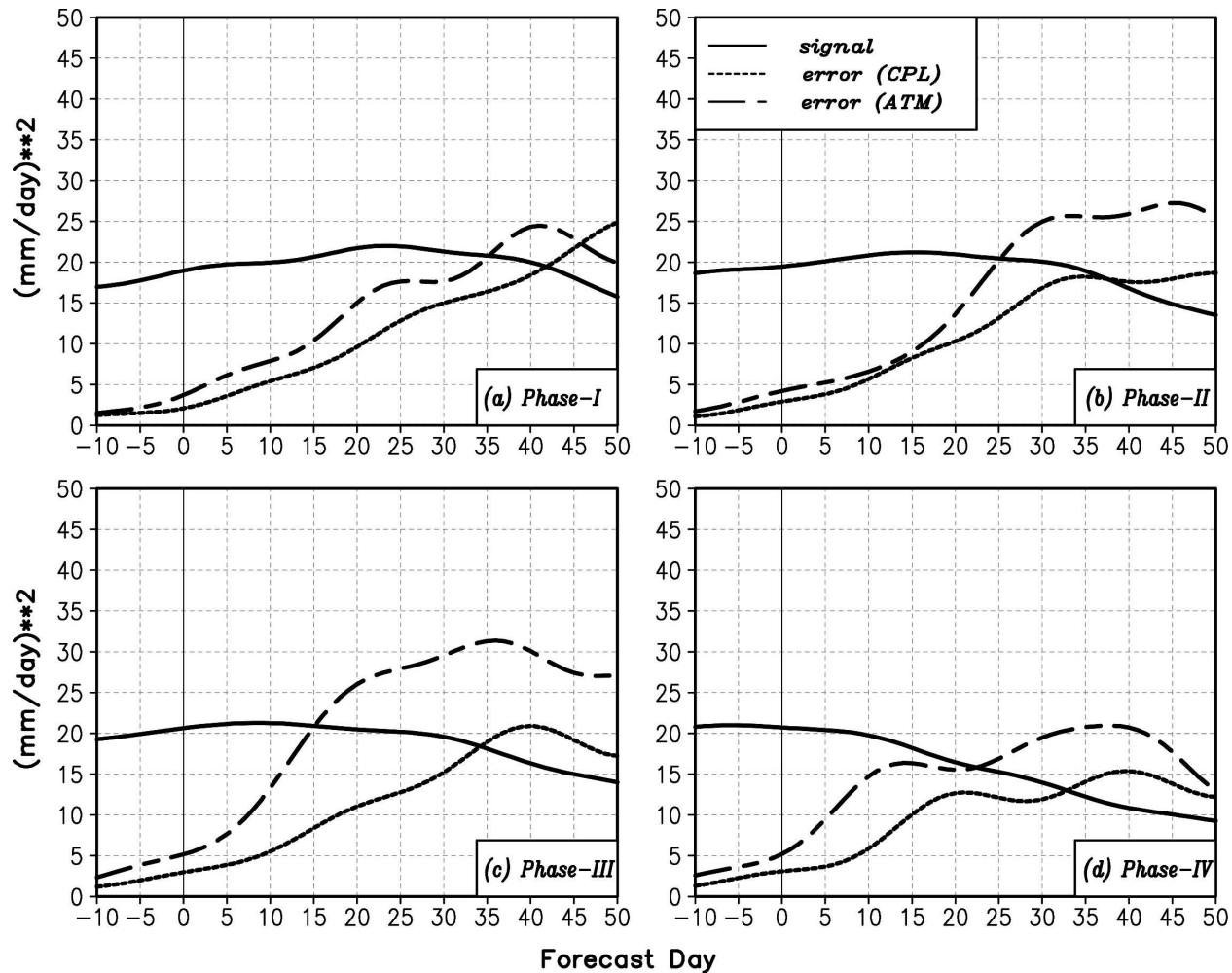
FIG. 2. The filtered signals and forecast errors averaged over Southeast Asia (10°–30°N, 65°–120°E) when forecasts start from phase (a) I (active), (b) II (active to break), (c) III (break), and (d) IV (break to active) with the coupled model (CPL) and atmosphere-only model (ATM). The data used to calculate the signals and errors are the filtered rainfall.

transition from the wet (dry) to dry (wet). For the coupled (atmosphere only) forecasts, the predictability from phases I to IV is, respectively, 41 (35), 35 (25), 34 (15), and 32 (22) days. Air–sea coupling extends the TISO predictability for all phases. The largest (smallest) extension occurs when forecasts start from the local break (active) condition (Figs. 2c,a). Because the break phase usually evolves into the active phase and vice versa, this result suggests that air–sea coupling particularly extends the TISO predictability for the active phase rather than that for the break phase over Southeast Asian region (Figs. 2c,a).

A relevant question worth being examined is as follows: Can air–sea coupling also extend weather predictability at the presence of TISO? To address this question, the signal and forecast error have been recalculated from daily model outputs (without using any

filtering). The signal is estimated as the variance of rainfall anomaly in the control run subject to 11-day running mean [instead of 51-day running mean for the TISO case (Waliser et al. 2003a)]. The rainfall anomaly is derived as the difference between the total daily rainfall and its four-month mean (two months before and after the forecast start date). The forecast error is the variance of the daily rainfall difference between the forecast and control run. Figure 3 shows the resultant weather signals and errors averaged over Southeast Asia when forecasts start from four different phases. When forecasts start from either active or break phases (Figs. 3a,c), air–sea coupling has no influence on Southeast Asian weather predictability. On the other hand, coupling seems to extend the weather predictability as forecasts start from the transition periods (Figs. 3d,b). In particular, when the forecasts start from the break-
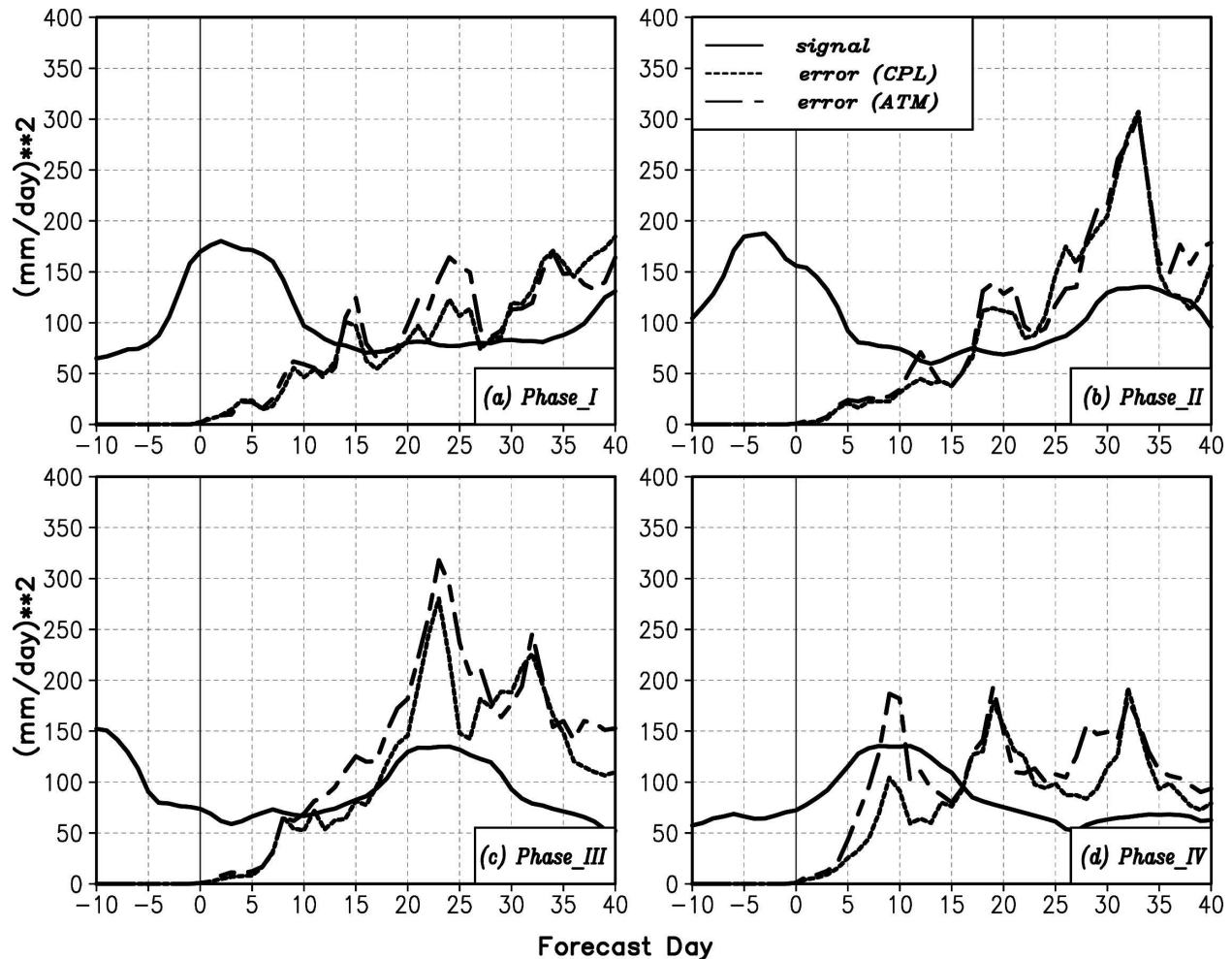
FIG. 3. The unfiltered signals and forecast errors averaged over Southeast Asia (10°–30°N, 65°–120°E) when forecasts start from phase (a) I (active), (b) II (active to break), (c) III (break), and (d) IV (break to active) with the coupled model (CPL) and atmosphere-only model (ATM). The data used to calculate the signals and errors are the unfiltered daily rainfall.

to-active transition (Fig. 3d), the forecast error in the coupled model is considerably reduced relative to that in the atmosphere-only model before day 15. The air–sea coupling, in this case, significantly extends the weather predictability over Southeast Asia by about a week. After examining other TISO active regions (e.g., the equatorial Indian Ocean, South China Sea, and western North Pacific), it is further confirmed that air–sea coupling tends to extend the weather predictability, particularly as the forecasts start from the break-to-active transition (figures not shown). Because the break-to-active transition is usually associated with positive SST anomaly, it is speculated that the extended weather predictability is primarily due to the regulation of the positive SST anomaly on the development of convection. To examine this hypothesis, two more experiments have been conducted in which only positive

(or negative) intraseasonal SST anomalies were included in the surface boundary conditions. Figure 4 shows the unfiltered signals and forecast errors from these two experiments, along with that from Fig. 3d. The forecast errors, when driven by the positive or negative SST anomalies, respectively, track those from the coupled run and atmosphere-only run during first 2 weeks. This result confirms that the extended weather predictability during the break-to-active transition is primarily due to the positive SST anomaly, which most likely exerts an external control on the convection movement.

b. Five different sea surface temperature configurations

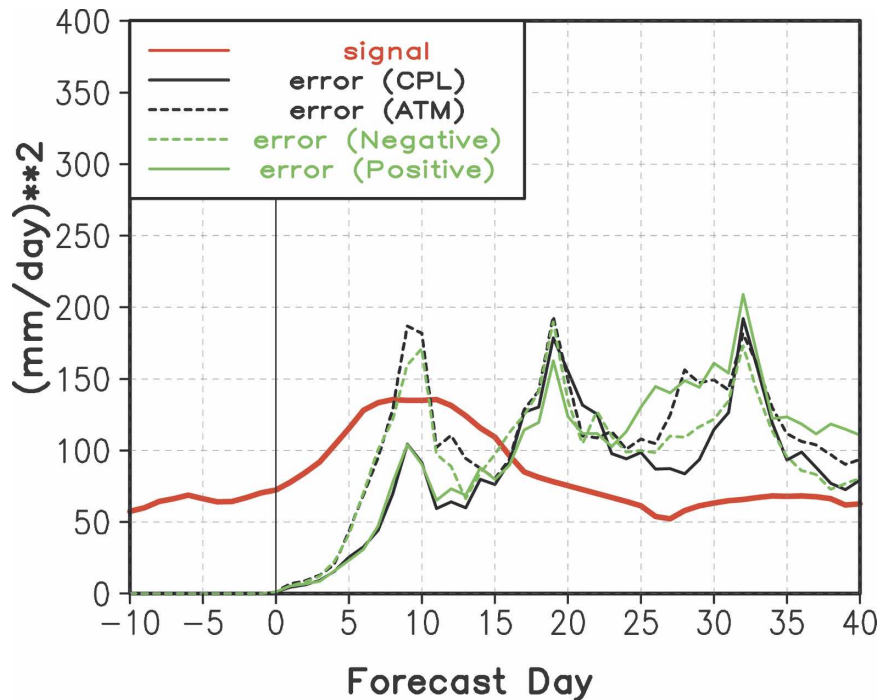Figure 5 summarizes the signals and forecast errors of rainfall averaged over Southeast Asia (10°–30°N,

FIG. 4. The unfiltered signals and forecast errors averaged over Southeast Asia (10°–30°N, 65°–120°E) when forecasts start during the break-to-active transition (phase IV in Fig. 3) with the coupled model (CPL) and atmosphere-only model (ATM), with a negative-only (Negative) and positive-only SST anomaly (Positive). The data used to calculate the signals and errors are the unfiltered daily rainfall.

65°–120°E) for five different SST boundary conditions. An example of the temporal evolution of five SSTs over the northern Indian Ocean is given in the appendix (Fig. A1). Under each SST setting (Table 1), 80 ensemble forecasts have been carried out. The error variance of an individual forecast is calculated from the difference between the forecast and the target. All 80 forecast errors are averaged with equal weighting to represent the forecast error under a specific SST setting. As usual, the TISO predictability is defined as the time when forecast error grows to reach the signal. The atmosphere-only forecasts driven by the "smoothed" SST (ATM) and damped persistent SST (ATMp) have the lowest predictability (~23 days). Coupling the atmospheric model to a slab mixed-layer ocean (ATMf) increases the predictability to 28 days. The highest predictability (~34 days) occurs when SST is directly produced by the full air–sea coupling (CPL). It is also very interesting to notice that the atmosphere-only model driven by the forecast daily SST[3] (ATMd) yields the

same predictability as that of the fully coupled case. This result seems inconsistent with a direct deduction from some previous studies (Fu et al. 2003; Fu and Wang 2004a; Zheng et al. 2004). They found that only the air–sea coupled system can sustain the observed quadrature rainfall–SST phase relationship, whereas the atmosphere-only model produces an almost in-phase SST–rainfall relationship. Thus, the TISO predictability of the atmosphere-only model even driven by "daily" SST should be significantly lower than that in the interactive air–sea coupled model (Fu and Wang 2004b; Waliser 2006). This issue will be addressed in section 4b.

Apart from using the signal-to-error ratio as a measure of TISO predictability, we also calculate the ACC between the rainfall anomaly in the ensemble forecast and that in the coupled control run over Southeast Asia (10°–30°N, 65°–120°E). For a specific SST configuration, the ACCs of all of the individual forecasts were calculated against the corresponding targets first. Then, the ACCs of a group of 80 forecasts were averaged to represent the ACC for that specific SST case. Figure 6 shows the ACCs as functions of forecast time for five different SSTs. The TISO predictability is defined as

---

[3] The 10-ensemble-mean daily SST (instead of individual ensemble SSTs) from the coupled forecasts has been used here.
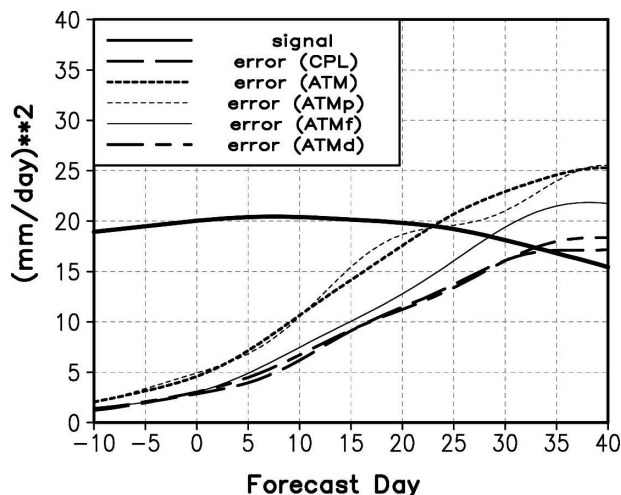
FIG. 5. The filtered signals and forecast errors averaged for all four phases over Southeast Asia (10°–30°N, 65°–120°E) under five different boundary conditions: (i) fully coupled air–sea model (CPL), (ii) atmosphere-only model forced by smoothed SST (ATM), (iii) atmosphere-only model forced by damped persistent SST (ATMp), (iv) atmosphere model coupled to a simple slab mixed-layer ocean model (ATMf), and (v) atmosphere-only model forced by daily SST (ATMd).
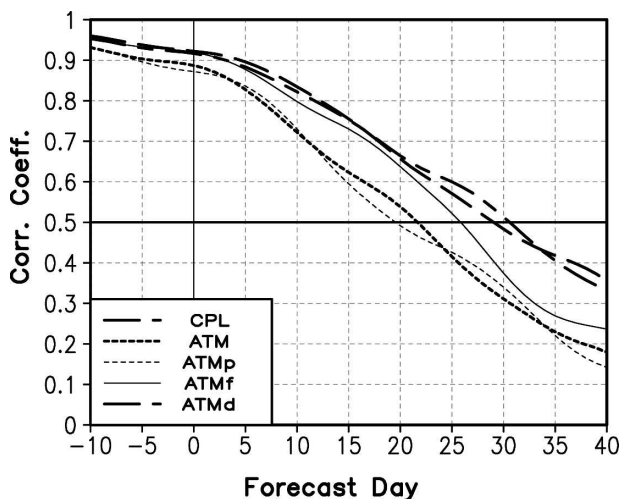

FIG. 6. The mean anomalous correlation coefficients for all four phase forecasts over Southeast Asia (10°–30°N, 65°–120°E) under five different boundary conditions: (i) fully coupled air–sea model (CPL), (ii) atmosphere-only model forced by smoothed SST (ATM), (iii) atmosphere-only model forced by damped persistent SST (ATMp), (iv) atmosphere model coupled to a simple slab mixed-layer ocean model (ATMf), and (v) atmosphere-only model forced by daily SST (ATMd).

the day when ACC drops to 0.5.[4] The resultant predictability is similar to that measured by the signal-to-error ratio (Fig. 5). The fully interactive air–sea coupled case (CPL) and the atmosphere-only case, driven by the forecast daily SST (ATMd), have the highest predictability (~30 days), followed by that case coupled to a slab mixed-layer ocean (~26 days, ATMf). The two atmosphere-only forecasts driven by smoothed SST (ATM) and damped persistent SST (ATMp) have the lowest predictability (~20 days). Generally speaking, two different measures of predictability yield very similar conclusions. Both of them suggest that the full air–sea coupling (CPL) generates the best SST boundary condition, which extends the TISO predictability by about 10 days over Southeast Asia relative to the uncoupled case (ATM).

In their pioneering works, Epstein (1969) and Leith (1974) suggested that the multiensemble mean should give a better forecast than a single realization because the ensemble mean provides a special, nonlinear filtering that reduces the growing errors. To examine the possible impacts of using ensemble means instead of individual forecasts on assessing the TISO predictability, we first averaged 10-ensemble forecasts starting at an individual phase and under a specific SST setting.

The ACC between the ensemble mean forecast and the target is then calculated. Finally, all ACCs (total 8 = 4 phases × 2 events) are averaged to represent the ACC for that specific SST case. Figure 7 summarizes the ACCs under five different SST configurations. Compared to the results derived with individual forecasts (Fig. 6), the TISO predictability after applying the ensemble mean has been uniformly extended by about 10 days for all five different SST configurations. This re-
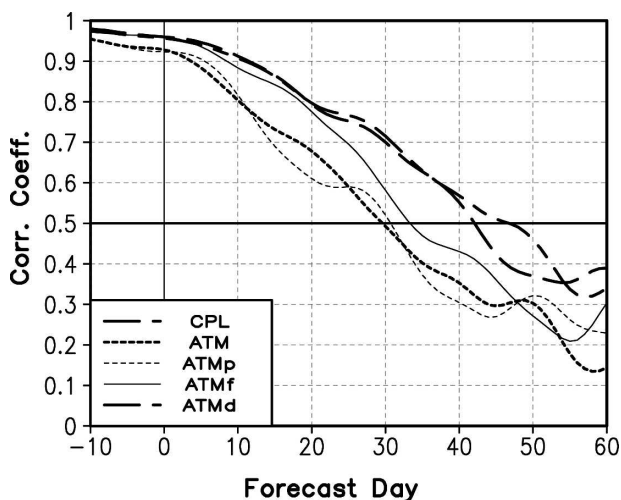

FIG. 7. As in Fig. 6, but the anomalous correlation coefficients are calculated using ensemble mean forecasts instead of individual ensembles.

---

[4] In a related study (Fu et al. 2007), we have shown that even when the ACC drops to 0.43, the forecast is still useful.

sult confirms the superiority of the ensemble mean over a single realization as the final product of TISO prediction.

4. SST feedback on extending the TISO predictability

The possible impacts of air–sea coupling on the evolution of TISO have been suggested by many observational studies (Krishnamurti et al. 1988; Zhang 1996; Hendon and Glick 1997; Lau and Sui 1997; Sengupta et al. 2001; Vecchi and Harrison 2002; Webster et al. 2002; Wang et al. 2005; Fu et al. 2006; Wang et al. 2006; etc.), and demonstrated by many modeling experiments (Sperber et al. 1997; Flatau et al. 1997; Wang and Xie 1998; Waliser et al. 1999; Kemball-Cook et al. 2002; Fu et al. 2003; Inness and Slingo 2003; Zheng et al. 2004; Sperber et al. 2005; Rajendran and Kitoh 2006; Zhang et al. 2006; Seo et al. 2007; Marshall et al. 2008; among others). The air–sea "*coupling*" implies a two-way interaction between the atmosphere and ocean. It is commonly accepted that the observed large-scale intraseasonal SST anomalies are primarily forced by surface heat and momentum fluxes associated with the TISO (Hendon and Glick 1997; Wang and Xie 1998; Sengupta and Ravichandran 2001; Waliser et al. 2004). However, whether and how the intraseasonal SST anomalies feed back to the TISO is still somewhat controversial (Hendon 2000; Zhang and Anderson 2003; Grabowski 2006). Two types of SST feedback mechanisms have been proposed in the literature. One suggests that intraseasonal SST anomalies feed back to the TISO through changing the atmospheric instability ahead of the convection (Lau and Sui 1997; Shinoda et al. 1998; Stephens et al. 2004; Fu et al. 2006). The other suggests that the feedback is through changing the boundary layer convergence (Wang and Xie 1998; Waliser et al. 1999; Fu and Wang 2004b; Seo et al. 2007).

For this particular model, the forecasts with intraseasonally varying SST in the boundary condition (CPL) have much longer TISO predictability than that without intraseasonal SST forcing (ATM; see Figs. 5,6). Because we used the same atmospheric model and initial conditions, the SST feedback processes that worked in the coupled case can be unraveled by analyzing the differences of the forecast rainfall and associated variables between these two cases. In particular, we will focus on those processes that have been recognized as important contributors to steering the northward propagation of the boreal summer TISO, for example, surface convergence (Wang and Li 1994), surface evaporation (Lau and Sui 1997; Shinoda et al. 1998; Fu

et al. 2006), and easterly vertical shear[5] (Jiang et al. 2004; Drbohlav and Wang 2005).

a. Feedback processes from sea surface temperature to the TISO

A case study will be conducted first to identify the possible links between intraseasonal SST and rainfall anomalies. Then, statistical analyses of all forecasts will be used to further examine these findings. All data used in this section are the unfiltered daily outputs from the coupled forecasts and atmosphere-only forecasts driven by smoothed SST. Event two (Fig. 1d) has been selected for the case study because the impact of air–sea coupling on the northward progression of TISO is particularly clear for this event. Figure 8 presents the latitude–time cross sections of the differences of rainfall, SST, surface convergence, and surface latent heat flux averaged over 65°–120°E between the coupled forecast and atmosphere-only forecast. Before day 25, the lead of the negative (positive) SST anomalies on the northward-propagating negative (positive) rainfall anomalies are very clear (Fig. 8a). In contrast, the reduced near-equatorial rainfall starting from day 12 is not obviously preceded by negative SST anomaly. Figure 8b shows that surface convergence (divergence) and positive (negative) rainfall anomalies are closely connected to each other, with the former slightly leading the latter; for example, the reduced near-equatorial rainfall is preceded by surface divergence. Figure 8c shows that the reduced latent heat flux (or evaporation) centered near 15°N at day 10 leads the sea surface warming, which in turn leads to increased surface evaporation. The positive (negative) SST anomalies, in general, also have a significant in-phase correlation with the enhanced (reduced) surface evaporation.

Figure 9 presents the corresponding differences in vertical structures of moisture and circulation, along with the associated surface anomalies between the coupled and uncoupled forecasts during the northward progression of TISO (primarily from days 10 to 25, as shown in Fig. 8a). On day 10 (Fig. 9a), the positive rainfall anomalies are near the equator, with a maximum around 2°S, whereas the positive SST and surface convergence anomalies are present in the Northern Hemisphere, with a maximum around 6°N. The surface convergence is probably initiated by an anomalous SST gradient, as suggested by Lindzen and Nigam (1987). The enhanced evaporation associated with a positive

---

[5] Easterly vertical shear usually indicates that the upper layer is easterly and the lower layer is westerly; therefore, the resultant U850hPa − U200hPa will be positive for easterly vertical shear.

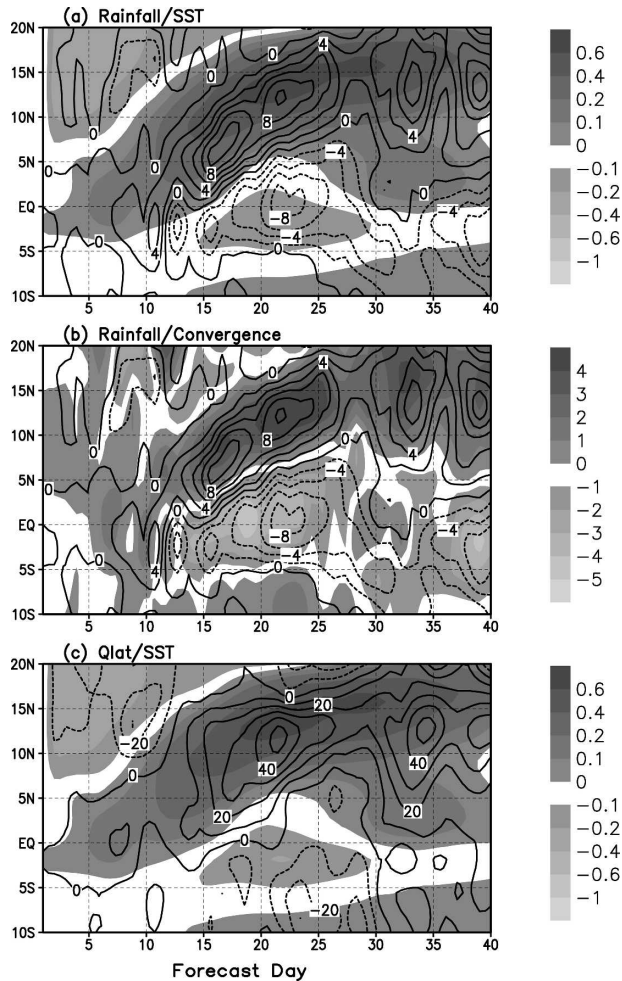FIG. 8. The latitude–time cross sections of the averaged differences over 65°–120°E between the coupled forecasts and atmosphere-only forecasts driven by smoothed SST for (a) rainfall (contours; interval of 2 mm day^{-1}) and SST (shading; °C), (b) rainfall (contours; interval of 2 mm day^{-1}) and surface convergence (shading; 1×10^{-6} s^{-1}), and (c) surface latent heat flux (contours; interval of 20 W m^{-2}, positive means upward) and SST (shading; °C). Both forecasts targeted event two (Figs. 1e,f) and started from phase I.

SST anomaly (the surface wind speed anomaly is almost zero) exists between the equator and 7°N. Both the surface convergence and evaporation contribute to the boundary layer moistening south of 10°N. North of 10°N, the surface moistening can be explained by the anomalous southward advection of moisture, as suggested by Jiang et al. (2004). Therefore, both the positive SST and surface convergence anomalies favor the rainfall anomaly propagating northward. On day 15, the maximum rainfall anomaly moves to 6°N, with maximum surface convergence, SST, and evaporation to the northern side. The surface moistening between 12° and 16°N can be attributed to the enhanced evaporation,

which in turn is due to the coexisting positive SST anomaly and enhanced surface winds. The near-equatorial surface divergence and reduced rainfall may be partly attributed to the subsidence of overturning meridional circulation. The potential roles of this overturning meridional circulation on monsoon dynamics have been pointed out by previous researches (e.g., Lau and Peng 1990; Annamalai and Sperber 2005). In this study, its implication on the TISO characteristics will be further discussed later.

On day 20 (Fig. 9c), the maximum rainfall moves to 9°N. Positive SST and surface convergence anomalies continue to lead the rainfall. The overturning meridional circulation is strengthened, which considerably dries the troposphere and increases (reduces) surface divergence (rainfall) near the equator. The enhanced evaporation to the north of 16°N indicates the direct contribution of local positive SST anomaly. On the other hand, the enhanced evaporation to the south of 5°N is likely caused by the intensified surface winds. On day 25 (Fig. 9d), the maximum rainfall anomaly propagates to 13°N and stays around this latitude for a while (Fig. 8a). The maxima of the positive SST, surface convergence, and evaporation anomalies are almost collocated with the maximum rainfall. The continuous buildup of surface moistening to the south of the convection suggests that the convection may move southward instead of northward, which did happen in a later period (Figs. 8a,b).

To further examine the possible SST feedback processes, the lag correlations of rainfall (or SST) differences between the coupled and uncoupled forecasts with a number of relevant variables are calculated. When rainfall anomaly is used as the reference time series, the domain-averaged (10°S–25°N, 65°–120°E) lag correlations between rainfall and SST, surface evaporation (Qlat), surface convergence (Conv), zonal wind vertical shear (U850hPa − U200hPa) (Shear), boundary layer air temperature (Ta), and humidity (Qa) are shown in Fig. 10. All of the time series used to calculate the lag correlations are from the differences of 90-day forecasts between the coupled and the uncoupled models (CPL and ATM in Table 1). The maximum SST anomaly appears about 5 days before the maximum rainfall anomaly. The maximum surface evaporation and convergence leads the rainfall by 2 days; the maximum boundary layer air temperature and humidity lead the maximum rainfall by about 1 day. The maximum easterly vertical shear, however, appears about 3 days after the maximum rainfall. These sequential relationships suggest that the positive SST anomaly enhances the surface evaporation and convergence, warming up and moistening the atmospheric boundary
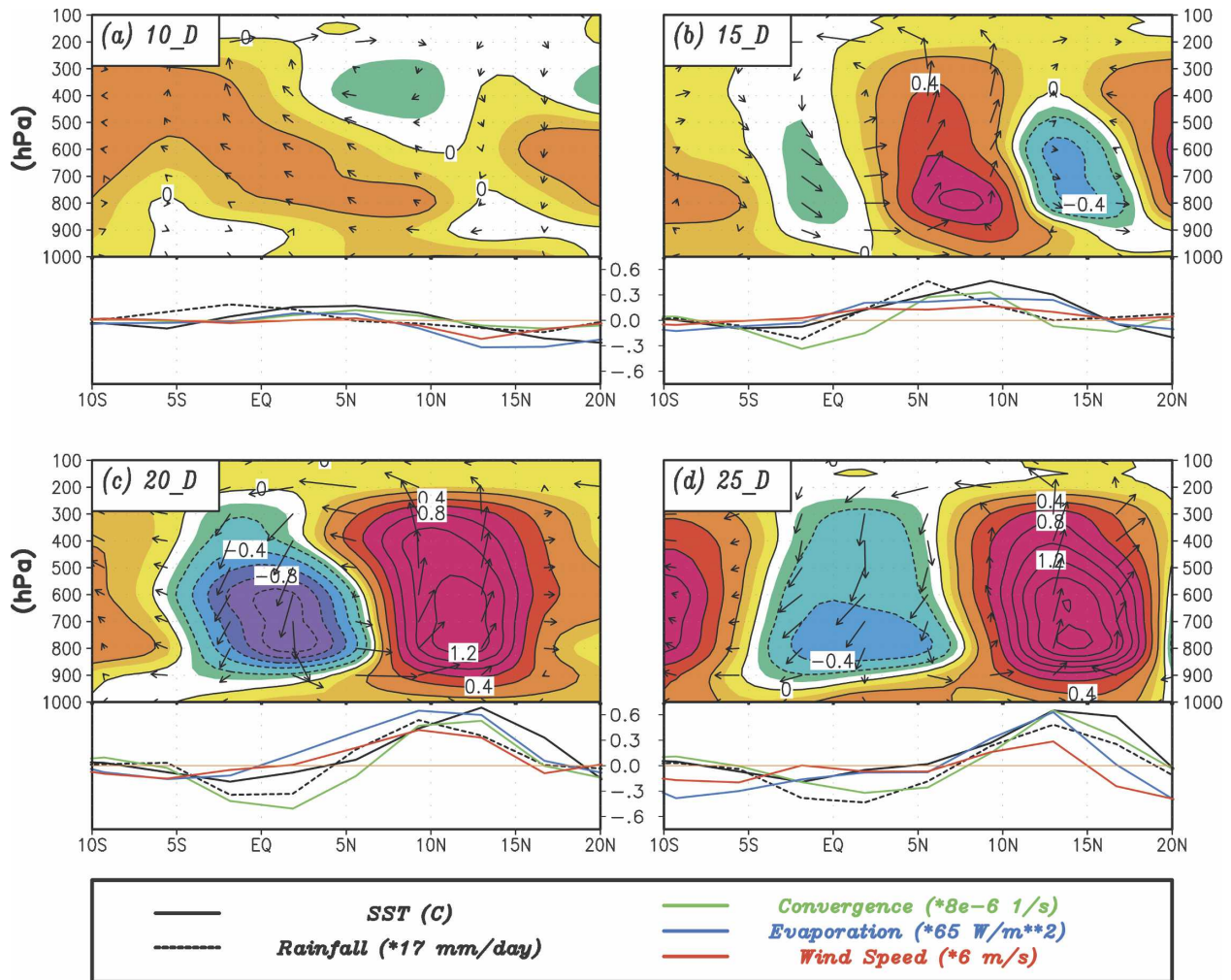
FIG. 9. (tops of panels) The vertical structures of the averaged differences of specific humidity (contours) and circulations (arrows) over 65°–120°E between the coupled forecasts and atmosphere-only forecasts driven by smoothed SST along with (bottoms of panels) the differences of SST (°C), rainfall (×17 mm day^{-1}), surface convergence (×8 × 10^{-6} s^{-1}), surface evaporation (×65 W m^{-2}), and wind speed (×6 m s^{-1}) at day (a) 10, (b) 15, (c) 20, and (d) 25. As in Fig. 8, both forecasts targeted event two (Figs. 1e,f) and started from phase I.

layer. All of these processes lead to the intensification of TISO-related convection, which further enhances the easterly vertical shear.

If the SST (rather than rainfall) anomaly is used as the reference time series, the resultant lag correlations between SST and rainfall (P), surface evaporation (Q_{lat}) and convergence (Conv), zonal wind vertical shear (U850hPa − U200hPa) (Shear), boundary layer air temperature (T_a), and humidity (Q_a) are given in Fig. 11. The maximum SST anomaly leads the surface convergence by ~1–2 days, suggesting that the positive SST anomaly directly induces surface convergence. However, the maximum correlation between SST and convergence is much smaller than that between convergence and rainfall. There are two possible causes: first,

part of the rainfall–convergence connection (Fig. 10) reflects the remote effect of the overturning meridional circulation (Fig. 9), rather than the direct effect of local SST; second, the interaction between anomalous convection and mean easterly shear is an important factor to enhance the surface convergence too (Jiang et al. 2004; Drbohlav and Wang 2005). The maximum SST anomaly leads the boundary layer air temperature and surface evaporation by about 2 days. The maximum correlation between SST and evaporation is much larger than that between the rainfall and evaporation. This further supports that the positive SST anomaly does enhance surface evaporation. The maximum rainfall appears about 5 days after the maximum SST. However, the maximum boundary layer humidity and east-
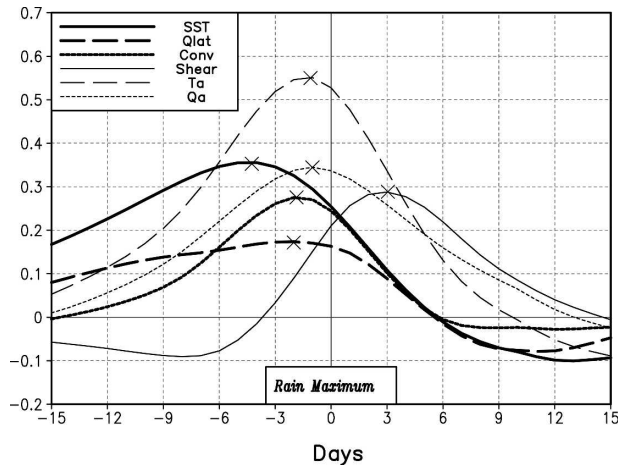
FIG. 10. The lagged correlations of differences of SST, surface latent heat flux (or evaporation, Qlat), surface convergence (Conv), zonal wind vertical shear (U850hPa − U200hPa, Shear), boundary layer air temperature (Ta), and specific humidity (Qa) referring to the rainfall differences between the coupled model (CPL) and atmosphere-only model (ATM) during 90-day forecasts for all four phases.

erly vertical shear occur even later. The late peak of boundary layer humidity in this case suggests that, in addition to the effect of SST, convection itself also plays important role in regulating the boundary layer humidity (e.g., Johnson 1980), which is an important issue that needs to be addressed in a future study.

From the above case study and statistical analyses, several important processes by which the SST anomaly
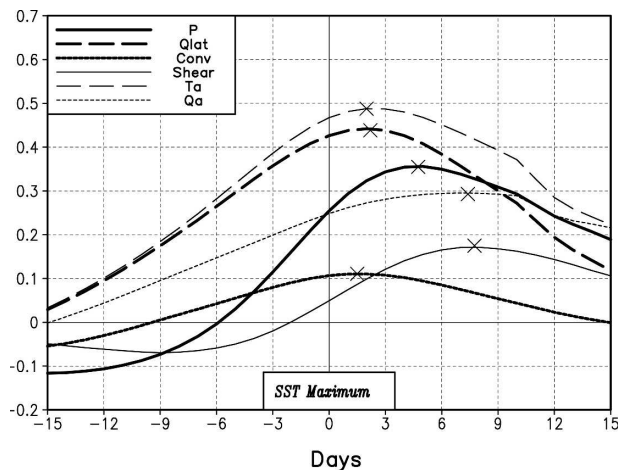

FIG. 11. The lagged correlations of differences of rainfall (P), surface latent heat flux (or evaporation, Qlat), surface convergence (Conv), zonal wind vertical shear (U850hPa − U200hPa , Shear), boundary layer air temperature (Ta), and specific humidity (Qa) referring to the SST differences between the coupled model (CPL) and atmosphere-only model (ATM) during 90-day forecasts for all four phases.

is manifest as a rainfall anomaly have been identified. A positive SST anomaly initiates anomalous convection by SST gradient-forced surface convergence, enhancing surface evaporation (Fig. 8) and warming up the atmospheric boundary layer (Figs. 10,11). The interaction between the anomalous convection and mean easterly shear also enhances the surface convergence (Jiang et al. 2004; Drbohlav and Wang 2005). The remote subsidence of overturning meridional circulation induced by the off-equatorial convection (Figs. 9b,c) reduces the near-equatorial convection, thus enhancing the northward pressure gradient and northward surface winds and further intensifying the off-equatorial convection.

Because the important role of mean easterly shear in the northward-propagating TISO has been emphasized by many previous studies (e.g., Wang and Xie 1996; Kemball-Cook et al. 2002; Jiang et al. 2004; Drbohlav and Wang 2005; Sperber et al. 2005; Ajayamohan and Goswami 2007), the enhanced northward-propagating TISO in the coupled forecast relative to the uncoupled case (Figs. 1,8) may be due to stronger mean easterly shear. Figure 12 examines the mean zonal wind vertical shears (U850hPa − U200hPa) as a function of latitude averaged during the first-month forecasts of two selected events (Figs. 1a,d). For event one (Fig. 12a), both forecast mean vertical shears are nearly the same, but are smaller than that of the control run in the Southern Hemisphere. In the Northern Hemisphere, the shear from the atmosphere-only forecast is even larger than that in the coupled forecast. For event two (Fig. 12b), the mean vertical shears from the control run, coupled forecast, and atmosphere-only forecast are nearly the same. Therefore, the enhanced northward-propagating TISO in the coupled forecasts cannot be attributed to the increase of mean easterly shear. We also compared the mean boundary layer humidity, which has been proposed by Ajayamohan and Goswami (2007) as a critical factor for the northward-propagating TISO in their numerical experiments. In our case, however, no significant difference of the mean boundary layer humidity is detected between the coupled forecast and atmosphere-only forecast (figure not shown). On the other hand, if we compare two selected TISO events, the easterly shear in event two (Fig. 12b) is systematically larger than that in event one (Fig. 12a), and so is the corresponding northward-propagating TISO (Figs. 1a,d). This result supports that the mean easterly shear plays an important role in steering the TISO northward in the Indo–western Pacific sector.

In the above analyses, we have suggested that the off-equatorial positive SST anomaly leads the enhanced rainfall, which in turn suppresses the convection near the equator through an overturning meridional circula-
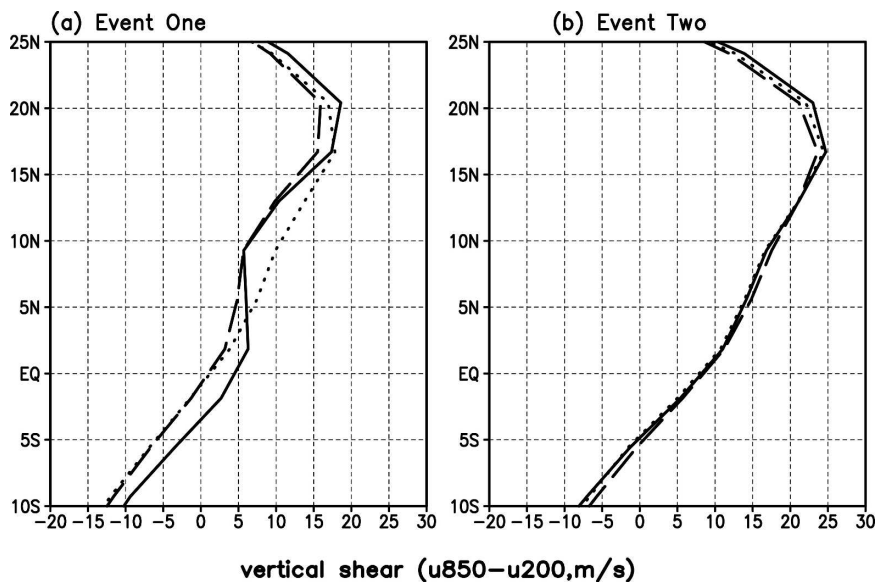
FIG. 12. The mean zonal wind vertical shear (U850hPa − U200hPa, m s^{-1}) averaged over 65°–120°E during the first 30-day forecasts from the control run (solid line), coupled run (CPL, long-dash line), and atmosphere-only run (ATM, dotted line) for event (a) one and (b) two.

tion. To examine whether this process works in the model, the lag regressions between the averaged SST anomaly in the Bay of Bengal (BoB; 10°–15°N, 80°–90°E) and the surface convergence anomaly over the globe have been calculated. Figure 13 shows the lag regressions with the surface convergence anomaly averaged over the equatorial and northern Indian Oceans. The maximum SST over the BoB leads surface
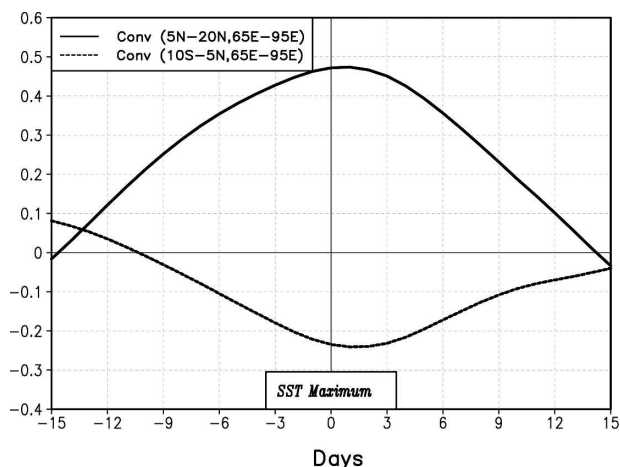

FIG. 13. The lag-regressed surface convergence differences (1 × 10^{-6} s^{-1}) over the northern (solid line) and equatorial (dotted) Indian Ocean referring to the SST differences over the Bay of Bengal (10°–15°N, 80°–90°E). The differences are derived between the coupled forecasts (CPL) and atmosphere-only forecasts (ATM).

convergence in the northern Indian Ocean by about 1–2 days, which in turn leads the equatorial surface divergence by another 1–2 days. This phase relationship supports that the northward-propagating positive SST anomaly leads the northward-propagating surface convergence and positive rainfall anomalies, which will generate subsidence near the equator through an overturning meridional circulation, acting to suppress the equatorial convection. This process has been confirmed by a sensitivity experiment with ECHAM4 AGCM (figure not shown). Figure 14 compares the autocorrelations of forecast daily rainfall anomalies (after removing the 3-month mean) in the coupled model and atmosphere-only model over the equatorial Indo–western Pacific Oceans. In the coupled model, the autocorrelation changes the sign from positive to negative at about 8–10 days. In the atmosphere-only model, the autocorrelation remains positive even after 15 days. This result suggests that active air–sea coupling may shorten the TISO period near the equator through enhancing the northward-propagating TISO and the associated overturning meridional circulation.

b. SST–rainfall relationship and atmospheric initial conditions

One interesting result shown in section 2 is that the TISO predictability in the atmosphere-only model (driven by forecast daily SST) is nearly the same as that in the air–sea coupled forecast (Figs. 5–7). This is dif-
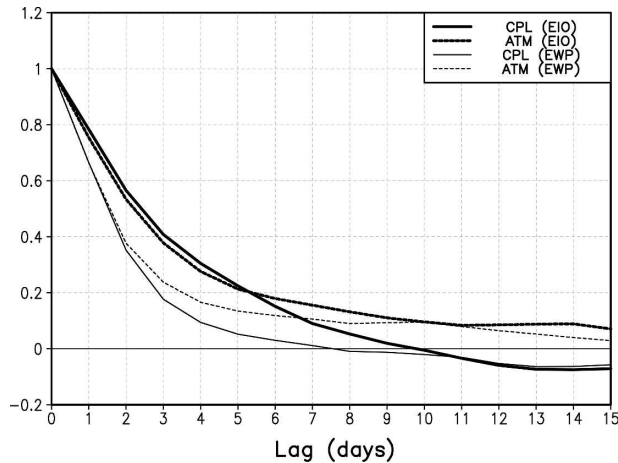
FIG. 14. Rainfall autocorrelations as a function of lagged days averaged in the EIO (5°S–5°N, 65°–95°E) and in the EWP (5°S–5°N, 120°–150°E) from the coupled forecasts (CPL, two solid lines) and atmosphere-only forecasts (ATM, two dotted lines).
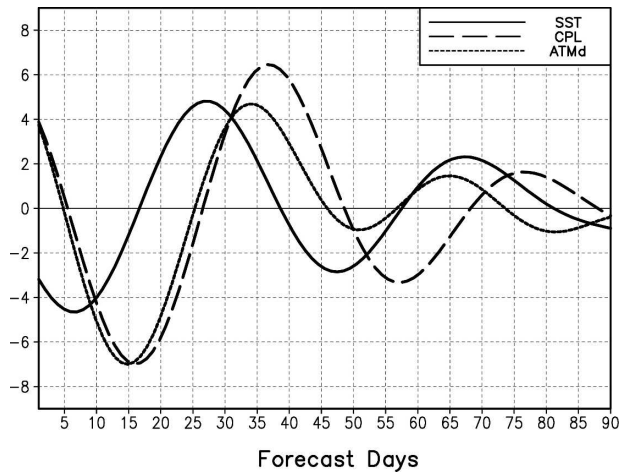

FIG. 15. The temporal evolutions of filtered SST and rainfall anomalies over the western Pacific (15°N, 150°E) from the coupled forecasts (CPL) and atmosphere-only forecasts driven by forecast daily SST (ATMd).

ferent from a direct deduction based on the results of previous free integrations (Fu and Wang 2004b; Waliser 2006), which suggested that the atmosphere-only run forced by daily SST cannot maintain the observed quadrature phase relationship between rainfall and SST, and thus the TISO predictability in the forced atmosphere-only forecast should be significantly lower than that in the coupled forecast (e.g., Wu et al. 2002; Fu et al. 2003; Zheng et al. 2004; Matthews 2004).

Apparently, current results turn out to be quite different from previous expectations. How do we reconcile this discrepancy? It can be explained by the different ways these experiments were conducted and different time periods in which SST–rainfall relationships were calculated. Under a forced atmosphere-only forecast setting (ATMd in Table 1), the initial atmospheric conditions contain significant intraseasonal information (e.g., atmospheric moistening/heating and associated large-scale circulations) that will exert a strong internal dynamic control on the development of SST-driven convection (Lau et al. 1997), thus maintaining a quadrature SST–rainfall phase relationship for a while. Suppose that initially a positive SST anomaly is located around 10°N with deep convection near the equator, and the overturning meridional circulation associated with the equatorial convection generates strong subsidence in the off-equatorial regions, particularly over the Northern Hemisphere during boreal summer. The subsidence can significantly delay the onset of convection over the positive SST anomaly around 10°N, resulting in a quadrature SST–rainfall phase relationship. Figure 15 illustrates this point by showing the temporal evolutions of the filtered 90-day forecast SST anomaly and

associated rainfall anomalies for the coupled forecast and the forced atmosphere-only forecast at 15°N, 150°E. During two TISO cycles, the rainfall anomalies in the coupled forecast always follow the SST with a 10-day lag. The atmosphere-only forecast rainfall tracks the coupled forecast very well only within the first month; later, the forecast rainfall tends to become in phase with the underlying SST anomaly.

Under a forced atmosphere-only free-run setting (e.g., Wu et al. 2002; Fu et al. 2003; Zheng et al. 2004; Matthews 2004), there are two possible reasons for the resultant in-phase SST–rainfall relationship. First, if the initial atmospheric conditions were randomly chosen, there will be no large-scale subsidence over the positive SST anomaly to delay the onset of SST-driven convection. The positive rainfall anomaly will occur quickly over the positive SST anomaly. Second, even if proper initial atmospheric conditions were used, the forced atmosphere-only rainfall forecasts can only maintain a quadrature phase relationship with underlying SSTs by about a month (Fig. 15). Later on, the rainfall anomalies tend to become collocated with the underlying SSTs. Because the lag correlations between rainfall and SST were usually calculated with year-long or multiyear integrations (Wu et al. 2002; Fu et al. 2003; Zheng et al. 2004; Matthews 2004), the resultant in-phase relationship between rainfall and SST should be expected.

To further corroborate the above arguments, another set of atmosphere-only forecasts driven by daily SST (same as that used in the ATMd, see Table 1) has been carried out (referred to as ATMd_ini later). In this case, the original atmospheric initial conditions have been replaced with an atmospheric status on the same
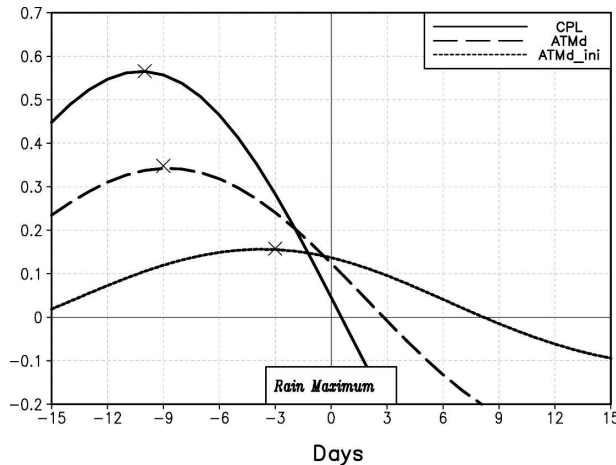
FIG. 16. The lagged correlations between the filtered SST and rainfall anomalies averaged over the northern Indian and western Pacific Oceans (5°–20°N, 65°–160°E) during 90-day forecasts for three different runs: the coupled run (CPL), the atmosphere-only run forced by daily SST (ATMd), and the atmosphere-only run forced by daily SST but with arbitrary initial conditions (ATM-d_ini).

calendar day, but from different integrations. Therefore, the new atmospheric initial conditions are no longer matched with the underlying SST at the beginning of the forecasts. The lag correlations between filtered SST and rainfall during 90-day forecasts from three runs (CPL, ATMd, and ATMd_ini) are compared. Figure 16 summarizes the domain-averaged lag correlations between rainfall and SST over the northern Indo–western Pacific Oceans (5°–20°N, 65°–160°E) for three 90-day forecasts (CPL, ATMd, and ATMd_ini). The maximum correlation coefficients for the three forecasts are, respectively, 0.57, 0.34, and 0.16. The leads from SST to rainfall are also reduced from 10 days in the coupled case to 3 days in the ATMd_ini case.

The above result indicates that the strongest coupling (highest correlation) between the intraseasonal SST and rainfall anomalies occurs in the coupled forecasts, with SST leading rainfall by about 10 days. Both correlation coefficients and lead days decrease in the atmosphere-only forecasts driven by daily SST. However, in the first month of the atmosphere-only forecast, the intraseasonal rainfall and SST are able to maintain the quadrature phase relationship, but quickly become in phase later. This result suggests that the reasonable matchup between atmospheric initial condition and underlying daily SST enables the atmosphere-only forecast to have a very similar predictability as that of the coupled forecast. If the atmospheric initial condition does not match up with the underlying daily SST, the resultant SST–rainfall relationship becomes nearly in phase, which is the same as that found in previous free integrations (Wu et al. 2002; Fu et al. 2003; Zheng et al. 2004; Matthews 2004).

5. Summary and discussion

To find the best SST configuration for the hindcasts and operational forecasts of the TISO (Waliser et al. 2003b; Fu et al. 2007), a series of ensemble forecasts have been conducted to quantify the TISO predictability under different SST conditions (Table 1). The five different lower boundary conditions, respectively, are as follows: (i) SST directly generated by full ocean–atmosphere coupling (CPL), (ii) smoothed SST from the coupled control run (ATM), (iii) damped persistent SST (ATMp), (iv) SST produced by anonymous coupling to a slab mixed-layer ocean model (ATMf), and (v) daily SST from the coupled forecast (ATMd). The following two complementary methods have been used to quantify the TISO predictability: (i) the ratio of signal to forecast error and (ii) the anomalous correlation coefficient (ACC). Because a "perfect" model assumption has been implied in this study, the predictability examined here is actually "potential" predictability rather than the "practical" predictability assessed in other studies (e.g., Seo et al. 2005; Woolnough et al. 2007).

The fully coupled atmosphere–ocean model has the highest predictability that reaches over 30 days (Figs. 5,6) averaged in Southeast Asia (10°–30°N, 65°–120°E). The atmosphere-only forecasts driven by "smoothed" and damped persistent SSTs have the lowest predictability (~20 days). The atmospheric model, after coupling to a slab mixed-layer ocean, achieves a predictability of about 25 days. It is also found that the atmosphere-only model, when driven by forecast daily SST, has nearly the same predictability as that of the fully coupled model. Further analysis indicates that the ensemble mean forecast has much higher skill than that of the individual forecasts. The ensemble mean forecast extends the TISO predictability by another 10 days under all boundary conditions (Fig. 7). The above findings suggest that fully coupled atmosphere–ocean model produces the best lower boundary condition for the TISO prediction. The atmosphere-only model, driven by the daily SST forecast by the coupled model (tier two), could reach the same skill as the directly coupled forecasts (tier one). Coupling a slab mixed-layer ocean to an atmospheric model also modestly increases the predictability relative to the atmospheric model forced by the smoothed and damped persistent SSTs.

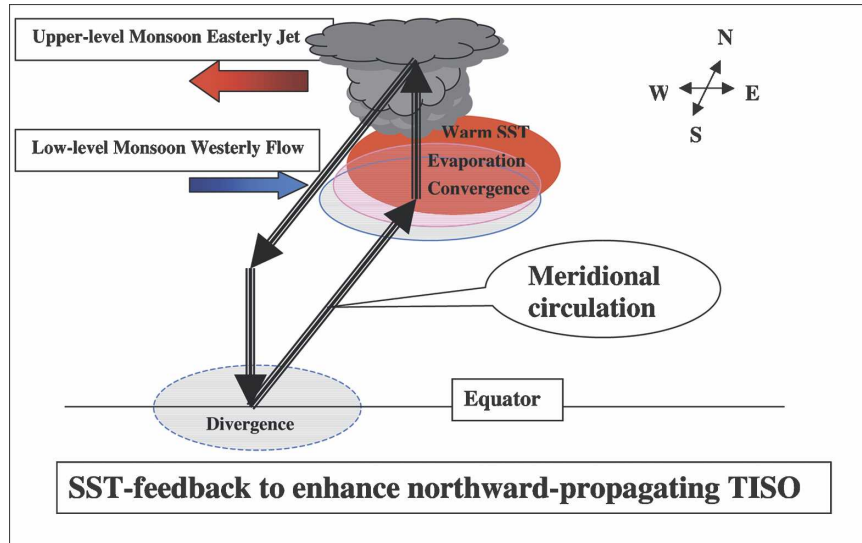For the Southeast Asian region (10°–30°N, 65°–

FIG. 17. A schematic shows the major ingredients involved in the SST feedback to enhance the northward-propagating tropical intraseasonal oscillation.

120°E), atmosphere–ocean coupling particularly extends the TISO predictability when the forecasts start from the break phase (Fig. 2). The break phase usually evolves into active phase, suggesting that the positive SST anomaly generated in the break phase (Sengupta and Ravichandran 2001; Fu et al. 2003) plays an important role during the onset of deep convection. It is also found that air–sea coupling significantly extends the weather predictability during the break-to-active transition (Fig. 3d). Two additional experiments, forced respectively by forecast daily SSTs that include only positive or negative intraseasonal SST anomaly, further corroborated that the positive SST anomaly, rather than the negative SST anomaly, is the key factor to extending the weather predictability (Fig. 4).

The major ingredients involved in the SST feedback processes for this model have been summarized in Fig. 17. The positive SST anomaly in the northern Indo–western Pacific Oceans increases the local evaporation and surface convergence (Figs. 8,9), which leads the positive rainfall anomaly propagating northward. The interactions between anomalous convection and mean easterly shear (Fig. 12) further enhance surface convergence and evaporation (Wang and Xie 1996; Jiang et al. 2004; Drbohlav and Wang 2005). The convection-driven overturning meridional circulation favors surface divergence near the equator, which in turn increases the northward pressure gradient and northward surface winds (Fig. 9), thereby intensifying the off-equatorial surface convergence and convective disturbances. The above scenario suggests that the final rainfall differences between the coupled and uncoupled

forecast is not just a linear atmospheric response to the underlying SST anomaly, as implied in previous studies (Lau and Sui 1997; Shinoda et al. 1998; Stephens et al. 2004; Fu et al. 2006). The SST feedback actually involves strong interactions between the convective disturbances and the mean state. The positive SST anomalies trigger the feedback processes through enhancing surface evaporation and surface convergence. In boreal summer, both the mean easterly shear and the overturning meridional circulation act as "amplifiers" of the SST feedback to the TISO. Therefore, the manifestation of air–sea coupling on the TISO depends not only on the magnitude and distribution of intraseasonal SST anomalies, but also on the atmospheric mean state.

Another interesting finding of this study is that the atmosphere-only model driven by forecast daily SST has nearly the same predictability as that of the coupled forecast (Figs. 5–7). This result is surprising because previous findings that an uncoupled model cannot sustain the observed quadrature SST–rainfall relationship (Fu et al. 2003; Zheng et al. 2004; Matthews 2004). Analysis of the uncoupled forecasts reveals that, during the first-month integration, the intraseasonal SST and convection anomalies are able to maintain the observed quadrature phase relationship (Fig. 15) because the internal dynamic/thermodynamic processes needed to delay the SST-driven convection have been included in the atmospheric initial conditions. Two reasons can explain the nearly in-phase SST–rainfall relationship derived from previous studies (Fu et al. 2003; Zheng et al. 2004; Matthews 2004). First, if arbitrary atmospheric

initial conditions that do not match the underlying daily SSTs were used, the resultant SST–rainfall relationship is almost in phase (Fig. 16). Second, even if the atmospheric initial conditions well match the underlying daily SST, using the model outputs from year-long or multiyear integrations will still result in the in-phase SST–rainfall relationship because the quadrature phase relationship can only be maintained within the first-month integration (Fig. 15).

The similar predictability between the coupled forecast and the uncoupled forecast driven by forecast daily SST indicates that, in principle, the so-called tier-one and tier-two systems (Goddard et al. 2001; Zheng et al. 2004) are both good strategies to forecast the TISO. This result also suggests that using observed high-frequency SSTs as boundary conditions is a proper choice for TISO hindcasts if the atmospheric initial conditions from the state-of-the-art reanalysis datasets (e.g., NCEP and European Centre for Medium-Range Weather Forecasts) are good enough to match the observed high-frequency SSTs. These hypotheses need to be examined in the context of hindcasts and real-time forecasts of TISO with the best available data and models. Our current findings further emphasized that, as a phenomenon with time scale between the weather forecast (~1 week) and climate outlook (>1 month), the successful prediction of TISO critically depends on the settings of both initial and boundary conditions. Last, because the number of cases and ensembles used in this study is very limited and some results may be model dependent, future studies with more cases and ensembles using different models are needed in order to reach community-wide consensus.

APPENDIX

An Example of SSTs in Five Sensitivity Experiments

The temporal evolution of SSTs averaged over 10°–15°N, 90°–95°E in five experiments (Table 1), along with that from the coupled control run, is given in Fig. A1. These results correspond to the forecasts starting from phase I of TISO event two (Fig. 1). In terms of
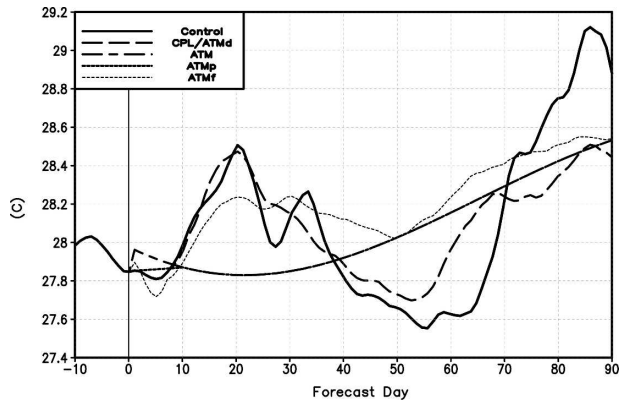

FIG. A1. Temporal evolutions of SSTs in the coupled control run (control), fully coupled (and daily) forecasts (CPL/ATMd), smoothed forecast (ATM), damped persistent forecast (ATMp), and coupling to a slab mixed-layer ocean (ATMf). The SSTs for the CPL/ATMd and ATMf runs are 10 ensemble means.

low-frequency variability, SSTs in the fully coupled (and daily) forecasts (CPL/ATMd) track that well in the coupled control run toward about 50 days. Coupling to a slab mixed-layer ocean (ATMf) underestimates the SST variability in the control run and coupled (and daily) forecasts. SSTs in the smoothed (ATM) and damped persistent (ATMp) runs are very similar, except that in the beginning the SST in the smoothed run has a discontinuity but has a gradual transition in the damped persistent run.

REFERENCES

Ajayamohan, R. S., and B. N. Goswami, 2007: Dependence of simulation of boreal summer tropical intraseasonal oscillations on the simulation of seasonal mean. *J. Atmos. Sci.,* **64,** 460–478.

Annamalai, H., and K. R. Sperber, 2005: Regional heat sources and the active and break phases of boreal summer intraseasonal (30–50 day) variability. *J. Atmos. Sci.,* **62,** 2726–2748.

Bessafi, M., and M. C. Wheeler, 2006: Modulation of south Indian Ocean tropical cyclones by Madden–Julian oscillation and convectively coupled equatorial waves. *Mon. Wea. Rev.,* **134,** 638–656.

Ding, Q. H., and B. Wang, 2005: Circumglobal teleconnection in the Northern Hemisphere summer. *J. Climate,* **18,** 3483–3505.

Donald, A., H. Meinke, B. Power, A. H. N. Maia, M. C. Wheeler, N. White, R. C. Stone, and J. Ribbe, 2006: Near-global impact of the Madden-Julian oscillation on rainfall. *Geophys. Res. Lett.,* **33,** L09704, doi:10.1029/2005GL025155.

Drbohlav, H.-K. L., and B. Wang, 2005: Mechanism of the northward-propagating intraseasonal oscillation: Insights from a zonally symmetric model. *J. Climate,* **18,** 952–972.

Epstein, E. S., 1969: Stochastic dynamic prediction. *Tellus,* **21,** 739–759.

Ferranti, L., T. N. Palmer, F. Molteni, and E. Klinker, 1990: Tropical-extratropical interaction associated with the 30–60 day

oscillation and its impact on medium and extended range prediction. *J. Atmos. Sci.,* **47,** 2177–2199.

Flatau, M., P. Flatau, P. Phoebus, and P. Niller, 1997: The feedback between equatorial convection and local radiative and evaporative processes: The implications for intraseasonal oscillations. *J. Atmos. Sci.,* **54,** 2373–2386.

Fu, X., and B. Wang, 2001: A coupled modeling study of the seasonal cycle of the Pacific cold tongue. Part I: Simulation and sensitivity experiments. *J. Climate,* **14,** 765–779.

——, and ——, 2004a: Differences of boreal summer intraseasonal oscillations simulated in an atmosphere–ocean coupled model and an atmosphere-only model. *J. Climate,* **17,** 1263–1271.

——, and ——, 2004b: The boreal-summer intraseasonal oscillations simulated in a hybrid coupled atmosphere–ocean model. *Mon. Wea. Rev.,* **132,** 2628–2649.

——, ——, and T. Li, 2002: Impacts of air–sea coupling on the simulation of mean Asian summer monsoon in the ECHAM4 model. *Mon. Wea. Rev.,* **130,** 2889–2904.

——, ——, ——, and J. P. McCreary, 2003: Coupling between northward-propagating intraseasonal oscillations and sea surface temperature in the Indian Ocean. *J. Atmos. Sci.,* **60,** 1733–1753.

——, ——, and L. Tao, 2006: Satellite data reveal the 3-D moisture structure of Tropical Intraseasonal Oscillation and its coupling with underlying ocean. *Geophys. Res. Lett.,* **33,** L03705, doi:10.1029/2005GL025074.

——, ——, D. E. Waliser, and L. Tao, 2007: Impact of atmosphere–ocean coupling on the predictability of monsoon intraseasonal oscillations. *J. Atmos. Sci.,* **64,** 157–174.

Gaspar, P., 1988: Modeling the seasonal cycle of the upper ocean. *J. Phys. Oceanogr.,* **18,** 161–180.

Goddard, L., S. J. Mason, S. E. Zebiak, C. F. Ropelewski, R. Basher, and M. A. Cane, 2001: Current approaches to seasonal-to-interannual climate predictions. *Int. J. Climatol.,* **21,** 1111–1152.

Goswami, B. N., and P. K. Xavier, 2003: Potential predictability and extended range prediction of Indian summer monsoon breaks. *Geophys. Res. Lett.,* **30,** 1966, doi:10.1029/2003GL017810.

——, R. S. Ajayamohan, P. K. Xavier, and D. Sengupta, 2003: Clustering of synoptic activity by Indian summer monsoon intraseasonal oscillations. *Geophys. Res. Lett.,* **30,** 1431, doi:10.1029/2002GL016734.

Grabowski, W. W., 2006: Impact of explicit atmosphere–ocean coupling on MJO-like coherent structures in idealized aquaplanet simulations. *J. Atmos. Sci.,* **63,** 2289–2306.

Han, W., P. Webster, R. Lukas, P. Hacker, and A. Hu, 2004: Impact of atmospheric intraseasonal variability in the Indian Ocean: Low-frequency rectification in equatorial surface current and transport. *J. Phys. Oceanogr.,* **34,** 1350–1372.

Hendon, H. H., 2000: Impact of air–sea coupling on the Madden–Julian oscillation in a general circulation model. *J. Atmos. Sci.,* **57,** 3939–3952.

——, and B. Liebmann, 1990: The intraseasonal (30–50 day) oscillation of the Australian summer monsoon. *J. Atmos. Sci.,* **47,** 2909–2924.

——, and J. Glick, 1997: Intraseasonal air–sea interaction in the tropical Indian and Pacific Oceans. *J. Climate,* **10,** 647–661.

——, B. Liebmann, M. Newman, J. D. Glick, and J. E. Schemm, 2000: Medium-range forecast errors associated with active episodes of the Madden–Julian oscillation. *Mon. Wea. Rev.,* **128,** 69–86.

Hollingsworth, A., K. Arpe, M. Tiedtke, M. Capaldo, and H. Savijarvi, 1980: The performance of a Medium-Range Forecast Model in winter—Impact of physical parameterizations. *Mon. Wea. Rev.,* **108,** 1736–1773.

Inness, P. M., and J. M. Slingo, 2003: Simulation of the Madden–Julian oscillation in a coupled general circulation model. Part I: Comparison with observations and an atmosphere-only GCM. *J. Climate,* **16,** 345–364.

Jiang, X., T. Li, and B. Wang, 2004: Structures and mechanisms of the northward propagating boreal summer intraseasonal oscillations. *J. Climate,* **17,** 1022–1039.

Jin, F.-F., 1996: Tropical ocean-atmosphere interaction, the Pacific cold tongue, and the El Niño-Southern Oscillation. *Science,* **274,** 76–78.

Johnson, R. H., 1980: Diagnosis of convective and mesoscale motions during phase III of GATE. *J. Atmos. Sci.,* **37,** 733–753.

Jones, C., D. E. Waliser, J.-K. E. Schemm, and W. K. M. Lau, 2000: Prediction skill of the Madden and Julian oscillation in dynamical extended range forecasts. *Climate Dyn.,* **16,** 273–289.

——, ——, K. M. Lau, and W. Stern, 2004: The Madden–Julian oscillation and its impact on Northern Hemisphere weather predictability. *Mon. Wea. Rev.,* **132,** 1462–1471.

Kemball-Cook, S., B. Wang, and X. Fu, 2002: Simulation of the ISO in the ECHAM4 model: The impact of coupling with an ocean model. *J. Atmos. Sci.,* **59,** 1433–1453.

Kessler, W. S., M. J. McPhaden, and K. M. Weickmann, 1995: Forcing of intraseasonal Kelvin waves in the equatorial Pacific. *J. Geophys. Res.,* **100,** 10 613–10 631.

Krishnamurti, T. N., D. K. Oosterhof, and A. V. Mehta, 1988: Air-sea interaction on the time scale of 30 to 50 days. *J. Atmos. Sci.,* **45,** 1304–1322.

——, M. Subramaniam, G. Daughenbaugh, D. Oosterhof, and J. H. Xue, 1992: One-month forecast of wet and dry spells of the monsoon. *Mon. Wea. Rev.,* **120,** 1191–1223.

Lau, K. M., and P. H. Chan, 1986: Aspects of the 40–50 day oscillation during the northern summer as inferred from outgoing longwave radiation. *Mon. Wea. Rev.,* **114,** 1354–1367.

——, and L. Peng, 1990: Origin of low frequency (intraseasonal) oscillations in the tropical atmosphere. Part III: Monsoon dynamics. *J. Atmos. Sci.,* **47,** 1443–1462.

——, and C.-H. Sui, 1997: Mechanisms of short-term sea surface temperature regulation: Observations during TOGA COARE. *J. Climate,* **10,** 465–472.

——, and D. E. Waliser, Eds., 2005: *Intraseasonal Variability of the Atmosphere–Ocean Climate System.* Springer, 474 pp.

——, H. T. Wu, and S. Bony, 1997: The role of large-scale atmospheric circulation in the relationship between tropical convection and sea surface temperature. *J. Climate,* **10,** 381–392.

Leith, C. E., 1974: Theoretical skill of Monte Carlo Forecasts. *Mon. Wea. Rev.,* **102,** 409–418.

Liess, S., D. E. Waliser, and S. D. Schubert, 2005: Predictability studies of the intraseasonal oscillation with the ECHAM5 GCM. *J. Atmos. Sci.,* **62,** 3320–3336.

Lin, J.-L., and Coauthors, 2006: Tropical intraseasonal variability in 14 IPCC AR4 climate models. Part I: Convective signals. *J. Climate,* **19,** 2665–2690.

Lindzen, R. S., and S. Nigam, 1987: On the role of sea surface temperature gradients in forcing low-level winds and convergence in the Tropics. *J. Atmos. Sci.,* **44,** 2418–2436.

Lorenz, E. N., 1982: Atmospheric predictability experiments with a large numerical model. *Tellus,* **34,** 505–513.

Madden, R. A., and P. R. Julian, 1972: Description of global-scale

circulation cells in the tropics with a 40–50 day period. *J. Atmos. Sci.,* **29,** 1109–1123.

Maloney, E. D., and D. L. Hartmann, 2000: Modulation of east North Pacific hurricanes by the Madden–Julian oscillation. *J. Climate,* **13,** 1451–1460.

Marshall, A. G., O. Alves, and H. H. Hendon, 2008: An enhanced moisture convergence–evaporation feedback mechanism for MJO air–sea interaction. *J. Atmos. Sci.,* **65,** 970–986.

Matthews, A. J., 2004: Atmospheric response to observed intraseasonal tropical sea surface temperature anomalies. *Geophys. Res. Lett.,* **31,** L14107, doi:10.1029/2004GL020474.

McCreary, J. P., and Z. J. Yu, 1992: Equatorial dynamics in a 2.5-layer model. *Progress in Oceanography,* Vol. 29, Pergamon, 61–132.

McPhaden, M. J., 2004: Evolution of the 2002/03 El Niño. *Bull. Amer. Meteor. Soc.,* **85,** 677–695.

Mo, K. C., 2000: Intraseasonal modulation of summer precipitation over North America. *Mon. Wea. Rev.,* **128,** 1490–1505.

Nordeng, T. E., 1994: Extended version of the convective parameterization scheme at ECMWF and their impact on the mean and transient activity of the model in the tropics. ECMWF Research Department Tech. Memo. 206, 41 pp.

Paegle, J. N., L. A. Byerle, and K. C. Mo, 2000: Intraseasonal modulation of South American summer precipitation. *Mon. Wea. Rev.,* **128,** 837–850.

Rajendran, K., and A. Kitoh, 2006: Modulation of tropical intraseasonal oscillations by ocean–atmosphere coupling. *J. Climate,* **19,** 366–391.

Reichler, T., and J. O. Roads, 2005: Long-range predictability in the Tropics. Part II: 30–60-day variability. *J. Climate,* **18,** 634–650.

Roeckner, E., and Coauthors, 1996: The atmospheric general circulation model ECHAM4: Model description and simulation of present-day climate. Max-Planck Institute for Meteorology Rep. 218, 90 pp.

Sengupta, D., and M. Ravichandran, 2001: Oscillations of Bay of Bengal sea surface temperature during the 1998 summer monsoon. *Geophys. Res. Lett.,* **28,** 2033–2036.

——, B. N. Goswami, and R. Senan, 2001: Coherent intraseasonal oscillations of ocean and atmosphere during the Asian summer monsoon. *Geophys. Res. Lett.,* **28,** 4127–4130.

Seo, K.-H., and Y. Xue, 2005: MJO-related oceanic Kelvin waves and the ENSO cycle: A study with the NCEP Global Ocean Data Assimilation System. *Geophys. Res. Lett.,* **32,** L07712, doi:10.1029/2005GL022511.

——, J.-K. Schemm, and C. Jones, 2005: Forecast skill of the tropical intraseasonal oscillation in the NCEP GFS dynamical extended range forecasts. *Climate Dyn.,* **25,** 265–284.

——, ——, W.-Q. Wang, and A. Kumar, 2007: The boreal summer intraseasonal oscillation simulated in the NCEP Climate Forecast System: The effect of sea surface temperature. *Mon. Wea. Rev.,* **135,** 1807–1827.

Shinoda, T., H. H. Hendon, and J. Glick, 1998: Intraseasonal variability of surface fluxes and sea surface temperature in the tropical western Pacific and Indian Oceans. *J. Climate,* **11,** 1685–1702.

Sikka, D. R., and S. Gadgil, 1980: On the maximum cloud zone and the ITCZ over Indian longitudes during the southwest monsoon. *Mon. Wea. Rev.,* **108,** 1840–1853.

Sperber, K. R., J. M. Slingo, P. M. Inness, and K. M. Lau, 1997: On the maintenance and initiation of the intraseasonal oscillation in the NCEP/NCAR reanalysis and the GLA and UKMO AMIP simulations. *Climate Dyn.,* **13,** 769–795.

——, S. Gualdi, S. Legutke, and V. Gayler, 2005: The Madden–Julian oscillation in ECHAM4 coupled and uncoupled GCMs. *Climate Dyn.,* **25,** 117–140.

Stephens, G. L., P. J. Webster, R. H. Johnson, R. Engelen, and T. L'Ecuyer, 2004: Observational evidence for the mutual regulation of the tropical hydrological cycle and tropical sea surface temperatures. *J. Climate,* **17,** 2213–2224.

Tiedtke, M., 1989: A comprehensive mass flux scheme for cumulus parameterization in large-scale models. *Mon. Wea. Rev.,* **117,** 1779–1800.

Timmermann, A., and F.-F. Jin, 2002: A nonlinear mechanism for decadal El Nino amplitude changes. *Geophys. Res. Lett.,* **29,** 1003, doi:10.1029/2001GL013369.

Tracton, M. S., and E. Kalnay, 1993: Ensemble forecasting at NMC: Practical aspects. *Wea. Forecasting,* **8,** 379–398.

Vecchi, G., and D. E. Harrison, 2002: Monsoon breaks and subseasonal sea surface temperature variability in the Bay of Bengal. *J. Climate,* **15,** 1485–1493.

Waliser, D. E., 2006: Predictability of tropical intraseasonal variability. *Predictability of Weather and Climate,* T. Palmer and R. Hagedorn, Eds., Cambridge University Press, 275–305.

——, K. M. Lau, and J. H. Kim, 1999: The influence of coupled sea surface temperatures on the Madden–Julian oscillation: A model perturbation experiment. *J. Atmos. Sci.,* **56,** 333–358.

——, W. Stern, S. Schubert, and K. M. Lau, 2003a: Dynamic predictability of intraseasonal variability associated with the Asian summer monsoon. *Quart. J. Roy. Meteor. Soc.,* **129,** 2897–2925.

——, S. Schubert, A. Kumar, K. Weickmann, and R. Dole, 2003b: Proceedings from a workshop on "Modeling, simulation, and forecasting of subseasonal variability." NASA/CP 2003-104606, Vol. 25, 62 pp.

——, R. Murtugudde, and L. E. Lucas, 2004: Indo-Pacific Ocean response to atmospheric intraseasonal variability: 2. Boreal summer and the Intraseasonal Oscillation. *J. Geophys. Res.,* **109,** C03030, doi:10.1029/2003JC002002.

——, and Coauthors, 2006: The Experimental MJO Prediction Project. *Bull. Amer. Meteor. Soc.,* **87,** 425–431.

Wang, B., and H. Rui, 1990: Synoptic climatology of transient tropical intraseasonal convection anomalies: 1975-1985. *Meteor. Atmos. Phys.,* **44,** 43–61.

——, and T. Li, 1994: Convective interaction with boundary-layer dynamics in the development of a tropical intraseasonal system. *J. Atmos. Sci.,* **51,** 1386–1400.

——, and X. Xie, 1996: Low-frequency equatorial waves in sheared zonal flow. Part I: Stable waves. *J. Atmos. Sci.,* **53,** 449–467.

——, and ——, 1998: Coupled modes of the warm pool climate system. Part I: The role of air–sea interaction in maintaining Madden–Julian oscillation. *J. Climate,* **11,** 2116–2135.

——, T. Li, and P. Chang, 1995: An intermediate model of the tropical Pacific Ocean. *J. Phys. Oceanogr.,* **25,** 1599–1616.

——, P. J. Webster, and H. Teng, 2005: Antecedents and self-induction of active-break south Asian monsoon unraveled by satellites. *Geophys. Res. Lett.,* **32,** L04704, doi:10.1029/2004GL020996.

——, P. Webster, K. Kikuchi, T. Yasunari, and Y. J. Qi, 2006: Boreal summer quasi-monthly oscillation in the global tropics. *Climate Dyn.,* **27,** 661–675.

Webster, P. J., and C. Hoyos, 2004: Prediction of monsoon rainfall and river discharge on 15–30-day time scales. *Bull. Amer. Meteor. Soc.,* **85,** 1745–1765.

——, and Coauthors, 2002: The JASMINE pilot study. *Bull. Amer. Meteor. Soc.,* **83,** 1603–1630.

Whitaker, J. S., and K. M. Weickmann, 2001: Subseasonal variations of tropical convection and week-2 prediction of wintertime western North American rainfall. *J. Climate,* **14,** 3279–3288.

Woolnough, S. J., F. Vitart, and M. A. Balmaseda, 2007: The role of the ocean in the Madden-Julian oscillation: Implications for MJO prediction. *Quart. J. Roy. Meteor. Soc.,* **133,** 117–128.

Wu, M. L. C., S. Schubert, I. S. Kang, and D. E. Waliser, 2002: Forced and free intraseasonal variability over the south Asian monsoon region simulated by 10 AGCMs. *J. Climate,* **15,** 2862–2880.

Yasunari, T., 1979: Cloudiness fluctuations associated with the Northern Hemisphere summer monsoon. *J. Meteor. Soc. Japan,* **57,** 227–242.

Zebiak, S. E., and M. A. Cane, 1987: A model El Niño–Southern Oscillation. *Mon. Wea. Rev.,* **115,** 2262–2278.

Zhang, C., 1996: Atmospheric intraseasonal variability at the surface in the tropical western Pacific Ocean. *J. Atmos. Sci.,* **53,** 739–758.

——, and S. Anderson, 2003: Sensitivity of intraseasonal perturbations in SST to the structure of the MJO. *J. Atmos. Sci.,* **60,** 2196–2207.

——, M. Dong, S. Gualdi, H. H. Hendon, E. D. Maloney, A. Marshall, K. R. Sperber, and W. Wang, 2006: Simulations of the Madden–Julian oscillation in four pairs of coupled and uncoupled global models. *Climate Dyn.,* **27,** 573–592.

Zheng, Y., D. E. Waliser, W. F. Stern, and C. Jones, 2004: The role of coupled sea surface temperatures in the simulation of the tropical intraseasonal oscillation. *J. Climate,* **17,** 4109–4134.